Applied Surface Science 490 (2019) 430–435

Contents lists available at ScienceDirect

Applied Surface Science

journal homepage: www.elsevier.com/locate/apsusc

Full length article

# CO desorption from nickel-decorated muscovite mica

K.W.B. Hunvik, A. Støvneng, B. Pacáková, S. Raaen*

*Physics Department, Norwegian University of Science and Technology (NTNU), N7491 Trondheim, Norway*

ARTICLE INFO

*Keywords:*
Muscovite mica
Ni nanoparticles
CO desorption

ABSTRACT

Adsorption and desorption of CO from Ni nanostructures deposited on muscovite mica substrates have been studied by TPD and characterized by XPS and AFM. In agreement with previous reports it is found that CO does not adsorb on the bare mica substrate. The desorption spectra depend strongly on the Ni coverage on the mica substrate. Three coverage regimes have been found; for low Ni coverage of approximately 0.2 monolayers a dominant desorption peak is found near 400 K. For medium coverage of approximately 0.6 monolayers three distinct peaks appear in the temperature region from 250 to 550 K. For higher Ni coverage of approximately 3 monolayers a single peak is observed near 550 K. The high temperature peak was assigned to desorption from terrace sites, the medium temperature peak was assigned to step sites, and the low temperature peak was argued to stem from lateral interaction between adsorbed CO species and possible sites with low coordination, e.g. kink sites. Desorption parameters have been extracted from the low temperature part of the desorption spectra. Anomalous low values for the vibrational prefactors were obtained in the case of low Ni coverage. This is argued to be due to dissociation of CO.

## 1. Introduction

The adsorption characteristics of gases on metal surfaces are structure sensitive since the bonding varies from adsorption sites like different crystalline facets as well as step and kink sites. Of particular interest in this regard is adsorption on nanoparticles where the number of different adsorption sites depends on the type and size of the clusters. A comprehensive understanding of such phenomena is important in the field of catalysis in order to optimize turnover rates and selectivity as well as to reduce deactivation of catalytic processes [1–3]. Nanoparticles in the size range from 1 to 20 nm exhibit large changes in structural and electronic properties which affect catalytic properties.

In this work, adsorption of CO on the surface of muscovite mica, which is a non-swelling clay, is studied by use of X-ray photoelectron spectroscopy (XPS), temperature programmed desorption (TPD), and atomic force microscopy (AFM). Muscovite mica is available in high-grade natural and synthetic forms and show good thermal stability up to a temperature of 900 K. Nickel was deposited on the mica substrates surfaces prior to adsorption of CO. This system may serve as a model system for studying doped clay surfaces by surface analytical tools. Nickel was chosen as dopant due to its catalytic properties [4], and carbon monoxide is often conveniently used as a model gas in studies of adsorption and desorption of carbon containing gases [5]. In addition, catalytic reactions involving CO are important in a number of technological applications, e.g. a recent study has shown that Ni-mica catalysts exhibit high catalytic activity and long-term stability of ammonia decomposition to $CO_x$-free $H_2$, so that hydrogen can be used as a clean fuel [6]. Other studies have shown that nickel supported catalysts are effective for CO methanation, which can be useful for carbon capture, energy storage and production of synthetic natural gas for use in biofuels [7,8].

The present experiments show that CO does not adsorb on clean mica for temperatures down to 110 K. Previous experiments have shown that a contamination layer is formed on mica by adsorption of CO or $CO_2$ when water is present and acting as a binding agent, and that mica cleaved in ultra-high vacuum (UHV) does not adsorb CO [9,10]. Therefore, the adsorption of CO on the samples of sub monolayer coverages of Ni on mica is likely to occur at or near the Ni atoms. Growth of Ni on muscovite mica has been investigated for different sub-monolayer coverages and temperature treatments. Desorption parameters have been estimated from the low temperature edge of the TPD spectra.

## 2. Experimental

The muscovite mica substrate was obtained from Goodfellow (potassium aluminosilicate sheet, 0.15 mm thick and 12 mm diameter, condition clear ruby), and was cleaved in vacuum by using the scotch

* Corresponding author.
*E-mail address:* sraaen@ntnu.no (S. Raaen).

https://doi.org/10.1016/j.apsusc.2019.06.073
Received 12 April 2019; Received in revised form 23 May 2019; Accepted 7 June 2019
Available online 12 June 2019

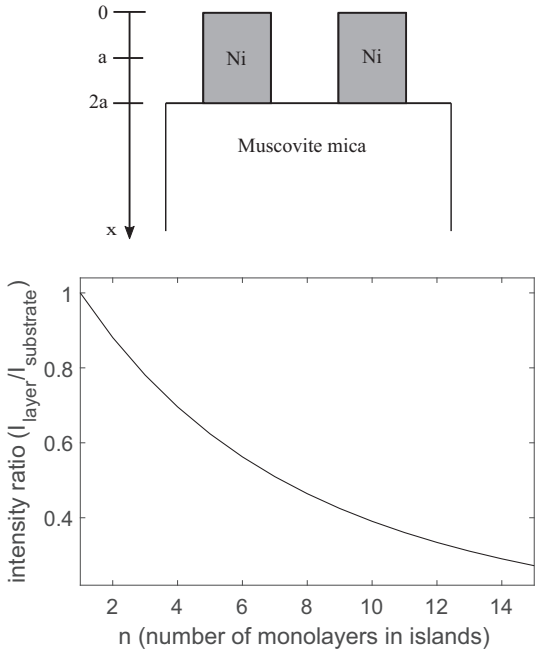


**Fig. 1.** Upper figure: Schematic diagram of a simplistic model of clustering on a surface, assuming two monolayers in the cluster. Lower panel: XPS layer/substrate intensity ratio as function of number of monolayers in the clusters (see text).

tape method. Subsequently, the mica was annealed overnight in UHV at a temperature of 700 K. Carbon contaminants were then removed by hydrogen gas bombardment using a naked filament placed in front of the sample and a hydrogen gas pressure of $2.6 \cdot 10^{-4}$ Pa at sample temperature 700 K. By measuring core level intensities by XPS before and after hydrogen treatment it was concluded that negligible changes in surface composition occurred caused by the treatment. The mica was mounted on a molybdenum support and was resistively heated. The sample could be cooled down to a temperature near 110 K. The surface structure of the cleaned mica surface was verified by low energy electron diffraction (LEED) to show a clear hexagonal pattern. Ni was deposited at the sample using thermal evaporation and e-beam deposition. A low evaporation rate of about 0.6 Å/min was used. The evaporation rate was verified by using a quartz crystal rate monitor as well as from XPS intensities. The effective thickness of the Ni layer after heating to 700 K was determined from core level intensities. A simplistic model of clustering is depicted in Fig. 1 for the case of two layers in the cluster. This model gives the following expression for the ratio of core level intensities $I_{layer}$ and $I_{sub}$ for layer and substrate:

$$\frac{I_{layer}}{I_{sub}} = \frac{\frac{\lambda_{layer}}{\lambda_{sub}}\left(1 - exp\left(-\frac{na}{\lambda_{layer}}\right)\right)}{n - 1 + exp\left(-\frac{na}{\lambda_{sub}}\right)}$$

where $a$ is the thickness of one monolayer, $\lambda_{layer}$ and $\lambda_{sub}$ are the electron mean free paths for core levels in layer and substrate, respectively, and $n$ is the number of monolayers in the cluster. TPD spectra were obtained by using a shielded and differentially pumped Prisma quadrupole mass spectrometer (Pfeiffer). The mass spectrometer was positioned close to the sample surface during measurements to discriminate against spurious desorption from the sample support, and to obtain reproducible intensities that could be compared for different runs. Simultaneous spectra were recorded from masses 2, 18, 28, 32 and 44 amu which correspond to $H_2$, $H_2O$, CO, $O_2$ and $CO_2$ molecules. XPS measurements were recorded using a SES2002 spectrometer (Scienta) in conjunction with a monochromatized Al K$\alpha$ X-ray source (Scienta). An energy resolution of about 0.4 eV was obtained at 200 eV pass

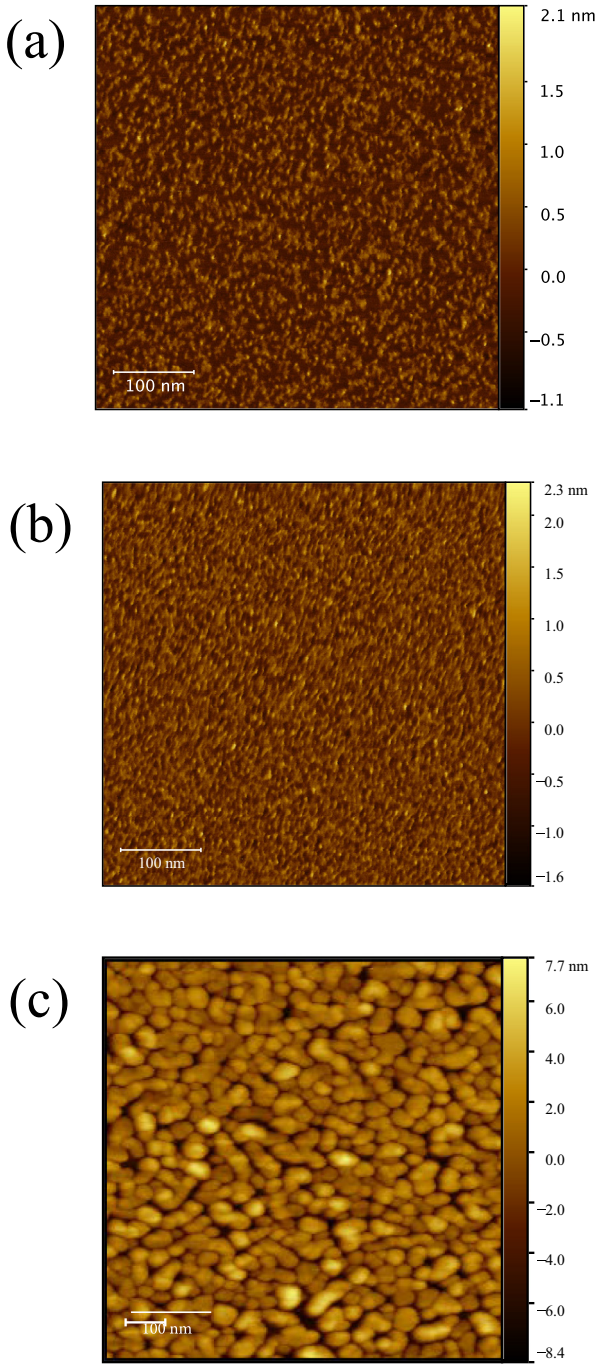


**Fig. 2.** AFM images of low, medium and large Ni coverage on muscovite mica. Effective Ni coverages are: (a) 0.1 ML, (b) 0.6 ML, and (c) 4.0 ML.

energy. A flood gun was used for charge neutralization during the photoemission measurements. AFM measurements were performed in the peak force-tapping mode in air, using a ScanAsyst probe on a Nanoscope IV microscope (Digital Instruments). The AFM images were recorded at atmospheric conditions after the TPDruns had been completed.

## 3. Results

AFM images are shown for low, medium and high Ni coverage in Fig. 2. These images were obtained in air after the samples had been removed from the UHV chamber after the TPD experiments had been performed. The coverage was estimated from XPS intensities that were

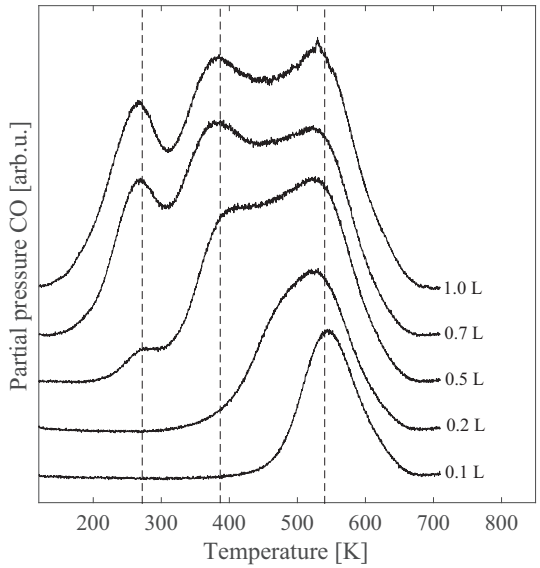


**Fig. 3.** TPD of CO from 0.56 ML Ni on mica. The CO exposure is given in the figure. Both Ni and CO were administered at a sample temperature of 150 K. Spectra are labelled by CO exposures 0.1, 0.2, 0.5, 0.7 and 1.0 L. The dashed lines indicate the position of the three major components of the spectra.

recorded after multiple temperature cycles. The line in the lower left corner of the images corresponds to 100 nm. The images in Fig. 2(a) and (b) are $500 \times 500\,nm^2$, whereas the image in Fig. 2(c) covers $1 \times 1\,\mu m^2$. The AFM images of the submonolayer Ni samples are similar in that the Ni structures have approximately the same diameter and height. The sample of medium Ni coverage, Fig. 2(b), appears to have a higher number of clusters packed closer together. The image from the large Ni coverage sample is quite different, Fig. 2(c). Larger Ni clusters are formed, both in diameter and height. It is worth noting that even for an effective coverage of 4 ML the Ni film is not continuous, as indicated by the fact the charge compensation was necessary to avoid peak distortion during XPS measurements.

Nickel was deposited onto vacuum-cleaved and hydrogen atom bombarded muscovite mica at coverage from 0.2 to 2.9 monolayers (ML). No carbon contaminants were observed by XPS on the clean mica surface. The substrate temperature was kept at 150 K during Ni deposition. Carbon monoxide was dosed at a temperature of 150 K at a partial pressure of $1.3 \cdot 10^{-6}$ Pa. It was found by TPD that no CO was adsorbed on the clean mica substrate down to 110 K. In Fig. 3 are shown TPD spectra of CO for a nickel coverage of 0.56 ML which was deposited at a substrate temperature of 150 K. The spectra are labelled by the CO dose; 0.1, 0.2, 0.5, 0.7 and 1.0 L (1 L = 1 Langmuir = $1.3 \cdot 10^{-4}$ Pa·s). The Ni coverage was estimated by XPS after the TPD runs were completed. The data in Fig. 3 are raw and unscaled data. Prior to the first TPD run, the sample was exposed to 1 L CO and heated by heating rate 1 K/s to 710 K. This was done to stabilize the Ni nanostructure.

From the TPD spectra, it was concluded that the saturation dose is near 1.0 L for CO dosed at 150 K. There are three distinct features in the desorption spectra at the higher CO exposures in Fig. 3; peaks are located in the temperature regions 250–280, 350–420, and 530–580 K. These TPD spectra are made complicated by assumedly several different adsorption sites as well as lateral interactions between adsorbed molecules. Kinetic parameters were obtained for the initial desorption by fitting the low temperature part using the Polanyi-Wigner equation [11]. The results are summarized in Table 1. Assuming molecular adsorption of CO the first order equation may be used. In Fig. 4 are shown fits to the leading edge of two of the spectra in Fig. 3. A linear background was subtracted from the spectra prior to the fitting procedure. The obtained desorption energies and vibrational pre-factors are shown

**Table 1**
Desorption parameters for different Ni coverage and CO exposure as described in the text, based on TPD spectra that were preheated to 710 K. Ni was deposited at 150 K, and CO exposures were done at 150 K substrate temperature. $E_d$ is the desorption energy and $\nu$ is the vibrational prefactor. The effective Ni coverage is given in monolayers.

| Ni coverage | CO exposure | $E_d$ | $\nu$ |
|---|---|---|---|
| [ML] | [L] | [eV] | [$s^{-1}$] |
| 0.20 | 0.1 | 0.31 | 301 |
| | 0.2 | 0.18 | 4 |
| | 0.4 | 0.14 | 1.1 |
| | 1.0 | 0.10 | 0.17 |
| 0.56 | 0.1 | 1.0 | $6.3 \cdot 10^7$ |
| | 0.2 | 0.42 | 110 |
| | 0.5 | 0.22 | 79 |
| | 0.7 | 0.17 | 13 |
| | 1.0 | 0.12 | 2 |
| 2.9 | 0.1 | 1.14 | $2.8 \cdot 10^8$ |
| | 0.5 | 0.92 | $8.7 \cdot 10^6$ |
| | 0.75 | 0.71 | $1.9 \cdot 10^5$ |
| | 1.0 | 0.61 | $2.2 \cdot 10^4$ |

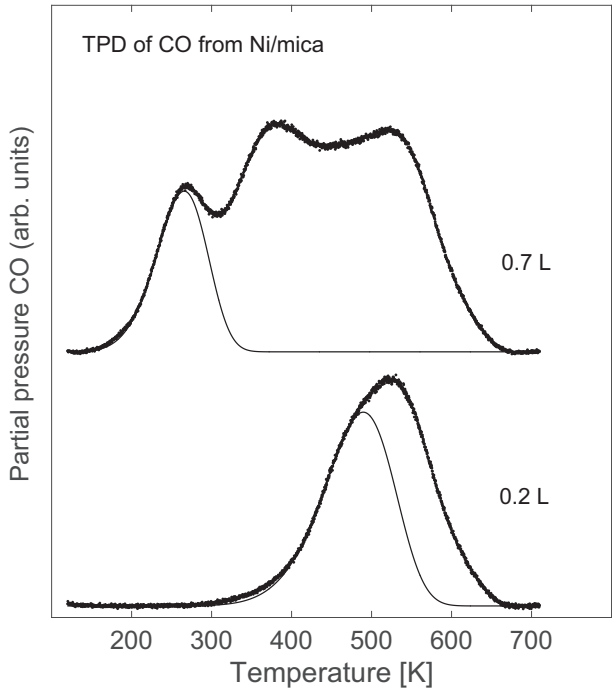


**Fig. 4.** TPD spectra from Fig. 3 showing fits to the low temperature part for CO exposures 0.2 L (bottom) and 0.7 L (top). First order desorption was assumed. Extracted desorption parameters are given in Table 1.

in Fig. 5 for the series of spectra in Fig. 3. The kinetic parameters depend on the coverage of CO and the assumption when extracting the parameters is that the coverage does not change more than a few percent for the region of the pre-edge that is being fitted [12]. Desorption energies were found to range from 1.0 (0.1 L CO exposure) to 0.12 eV (1.0 L CO exposure), and vibrational prefactors range from $6.3 \cdot 10^7$ to $2.0\,s^{-1}$.

In Fig. 6 is shown TPD data for CO adsorbed on 0.20 ML Ni on mica. Ni was deposited and CO was dosed at a substrate temperature of 150 K. A rearrangement of deposited Ni takes place during the first temperature run from 150 to 700 K. For subsequent runs the Ni/mica system seems unchanged as witnessed by reproducible desorption spectra. The spectra in Fig. 6 show runs where the CO doses range from 0.1 to 1.0 L, as indicated in the figure. A main peak is observed in the temperature

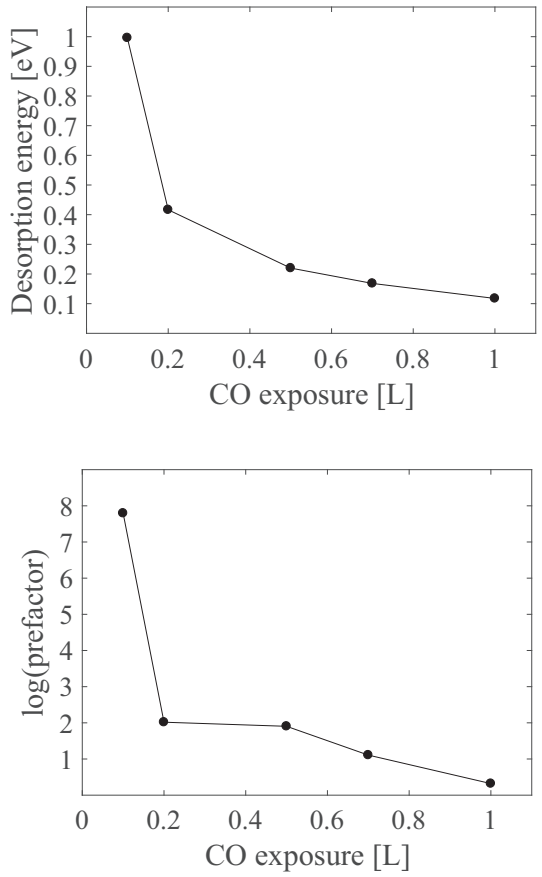


**Fig. 5.** (Upper curve) Desorption energy, and (Lower curve) log(prefactor) as functions of CO exposure, as obtained from analysis of the TPD spectra in Fig. 3.

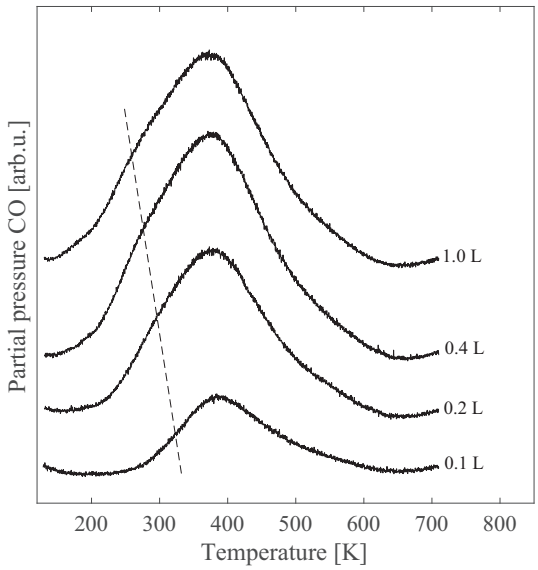


**Fig. 6.** TPD of CO from 0.20 monolayer Ni on mica. The CO exposure is given in the figure. Both Ni and CO were administered at a sample temperature of 150 K. Spectra are labelled by CO exposures 0.1, 0.2, 0.4 and 1.0 L. The dashed line indicates the low temperature shoulder that emerges with increases exposure to CO.

region from 370 to 400 K. For the highest exposures, 0.4 and 1.0 L, a low temperature shoulder of the main peak emerges. A relatively weak high temperature shoulder near 550 K is seen in all these spectra. Desorption parameters for the four bottom TPD spectra in Fig. 6 were found to range from 0.31 (for 0.1 L CO exposure) to 0.10 eV (for 1.0 L CO exposure) for the desorption energy, and from 301 to 0.17 $s^{-1}$ for the vibrational prefactor.

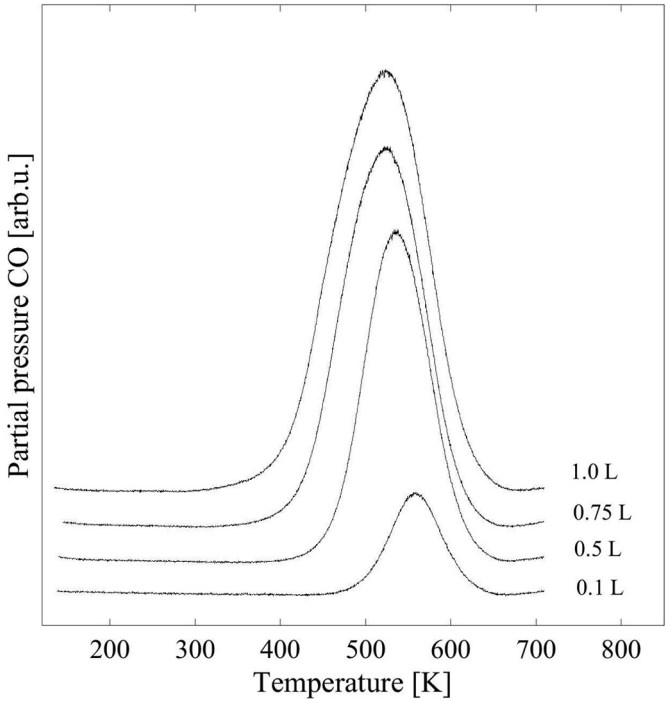


**Fig. 7.** TPD of CO from 2.9 monolayer Ni on mica. The CO exposure is given in the figure. Both Ni and CO were administered at a sample temperature of 150 K. Spectra are labelled by CO exposures 0.1, 0.5, 0.75 and 1.0 L.

For larger Ni depositions the TPD spectra are dominated by a high temperature desorption in the range 520 to 570 K. Fig. 7 shows TPD spectra from CO exposures 0.1, 0.5, 0.75 and 1.0 L, as indicated in the figure. For these spectra, 2.9 ML nickel was deposited at 150 K and CO was dosed at 150 K. For the lowest CO exposure (bottom curve), the peak appears near 560 K. The position of this peak moves to lower temperature with increased CO dose, and is located near 530 K for a CO exposure of 1.0 L. This shift and a broadening of the spectrum seem to be caused by a low temperature shoulder that appears with increased exposure, and which is not clearly resolved. Monte-Carlo simulations have previously showed that peaks at lower temperature appear with increasing CO coverage [13–15] due to lateral interactions between CO molecules. An analysis of the spectra as described above, results in desorption parameters where the desorption energy ranges from 1.14 (for 0.1 L CO exposure) to 0.61 eV (for 1.0 L CO exposure), and where the vibrational prefactor ranges from $2.8 \cdot 10^8$ to $2.2 \cdot 10^4$ $s^{-1}$. The obtained desorption parameters for low (0.2 ML), medium (0.56 ML) and high (2.9 ML) Ni coverage are summarized in Table 1.

## 4. Discussion

It is observed that the morphology of the nickel decorated muscovite mica surface changes with the initial temperature cycle from 130 to 710 K. Subsequent TPD cycles after the initial temperature run were found to be identical for the same exposure, thereby indicating that the morphology of the sample stays unchanged after the initial annealing to 710 K. The largest initial changes are observed for the largest Ni coverage. For the largest Ni coverage an effective thickness of 12.7 ML was estimated from XPS core level intensities prior to heating and 4.0 ML after heating. For the smallest Ni coverage a change from 0.1 to 0.08 ML was estimated. These changes may be understood in terms of clustering of Ni on the mica surface as the temperature is increased. The AFM images in Fig. 2 confirms that clustering of Ni takes place on the

mica substrate. In view of the relatively low temperature during heating cycles, evaporation and intercalation of Ni in the layered structure of muscovite mica are expected to be of less importance for the observed reduction of Ni intensities in the XPS core levels.

Three main desorption peaks around 250–280, 350–420, and 550–600 K are observed for CO desorption from Ni-mica samples having varying amounts of Ni on the surface. The samples with a small amount of nickel show one main peak around 400 K, the samples with medium amount of nickel show all three dominant features, whereas the samples with large amount of nickel show one desorption peak around 550 K, when the temperature rate was 1 K/s. An assignment of the various features in the desorption spectra may be based on previous reported findings [16,17]. The desorption peak near 250–280 K is assumed to be caused by dipole-dipole interaction between adsorbed CO molecules for large CO exposures when the distance between adsorbed molecules become small [13–15]. Reference to CO adsorbed on stepped Ni surfaces is relevant, as particulate Ni films may be expected to behave similar to stepped surfaces with regard to adsorption [18]. Earlier studies conducted by Benndorf and Meyer [16,17] show that the CO-Ni bonding strength was lowered for CO adsorbed on step sites. They assumed that the low temperature peaks in the CO desorption spectra were caused by adsorption on step sites. They also found a sequential filling of different desorption states with increasing CO coverage, similar to the present results obtained for the medium coverage Ni-mica surfaces. The Ni(111) surface only have one desorption peak near 450 K, whereas the stepped surfaces have several desorption peaks. For Ni(331) desorption peaks were reported at 455, 360 and 218 K, and for Ni(221) peaks were at 455, 300 and 250 K [16,17]. The high temperature desorption peak for the stepped surfaces was assumed to be due to adsorption on terrace sites. The fact that the position of desorption peaks in TPD depends on the heating rate complicates direct comparison between peak temperatures from different data sets; higher heating rate gives higher temperature for the peak position.

Since the present experiments do not determine the detailed structure of the Ni clusters on mica, the interpretation of the TPD data is based on the tendency of FCC metals to form clusters of the cubo-octahedral shape to minimize the free energy [19,20]. For cubo-octahedral clusters the number of terrace, step and kink sites varies with the size of the cluster. The recent work by de Araujo Filho and Murzin [21] shows that the fraction of terrace sites increases with the size of the cluster. For small clusters the fraction of terrace atoms approaches zero, whereas the terrace fraction for clusters consisting of few hundred atoms is more than 50%. In a real system, nanoparticles may have a variety of different shapes, however, the assumption that the fraction of terrace sites increase with cluster size seems reasonable.

Based on the above considerations, the assumption is that in the present data, the desorption peak around 550 K corresponds to desorption from terrace sites, and the peak near 400 K corresponds to desorption from step sites. Since the samples with several monolayers of Ni only have one peak near 550 K, the adsorption might only take place at terrace sites on top of large Ni clusters. For the mica samples with small amounts of nickel the fraction of terrace sites is small, and CO adsorption is predominantly on step sites, which gives a desorption peak near 400 K. For the samples with medium doses of Ni there may be a combination of step and terrace sites, and both peaks appear in the spectra. This interpretation is supported by the AFM images, in which nanostructures are observed at low Ni coverage (Fig. 1a and b), whereas distinct Ni nanoparticles are seen at higher coverage (Fig. 1c). The low temperature peak near 250 K is thought to be due to lateral interactions of adsorbed CO as the CO exposure is increased, but can also be due to adsorption on lower coordinated sites, e.g. kink sites and Ni sites at the Ni-mica interface. A comparison between the 0.56 ML (Fig. 4) and 0.2 ML (Fig. 6) samples shows a more distinct low temperature feature in the case of the 0.56 ML sample for 1 a CO exposure of 1.0 L. This is speculated to be caused more disordered Ni nanostructures in the case of the more dilute 0.2 ML sample, which leads to broader desorption features. The resolution of the AFM images is not high enough to confirm this point. The present results are consistent with previous results on adsorption of CO on Ni on glass [22], where desorption peaks near 170, 320, and 470 K were observed. The work by de Araujo Filho and Murzin [21] models TPD spectra from nanoparticles, and demonstrate how three-dimensional aspects of metal nanoclusters affect the TPD spectra. The obtained modelled spectra for ammonia on supported Pt particles are qualitatively similar to what is presently observed for CO on Ni-decorated mica [21].

A range of different adsorption sites exists on the Ni nanostructures. For the larger particles, terrace, edge and kink sites may predominate. For the smaller nanostructures the interface to the mica substrate may become increasingly important, and a range of low-coordinated sites may be present. Each TPD spectrum is therefore composed of several adsorption sites of different kinetic parameters. Due to the relative complexity of the TPD spectra, only kinetic parameters from the low temperature edge of the spectra have been extracted. These then represent the onset of desorption of CO from each sample. The desorption parameters as obtained from the TPD spectra are presented in Table 1. These parameters are believed to represent the range of kinetic parameters that exists in the Ni-mica samples. The results show unusual low vibrational prefactors $\nu$ for first order desorption where molecular adsorption is assumed. Typical values for $\nu$ in this case are of the order of $10^{13}\,s^{-1}$. Values of $\nu$ up to about $10^{8}\,s^{-1}$ were obtained for high Ni coverage and low CO exposure. For low amounts of Ni and high CO exposure values of $\nu$ below $1\,s^{-1}$ were found. These findings may not be consistent with the assumption of molecular adsorption on the Ni-mica system. The lower than expected estimated values for $\nu$ may be due to partly dissociation of CO on these surfaces. This may also partly be due to that the desorption spectra is composed by several peaks of near equal desorption parameters due to variety of near equivalent adsorption sites on the muscovite mica substrates. Indication of CO decomposition on these samples is given by XPS where a C 1s signal is measured after CO adsorption and subsequent TPD runs. However, readsorption of CO from the ambient vacuum on these very reactive Ni nanostructures cannot be ruled out. Earlier work of CO adsorption on Ni surfaces show the tendency that CO dissociates on the surface of Ni in the presence of an electron beam for LEED and Auger experiments [23,24]. The previous work by Doering, Dickenson, and Poppa [18] showed that CO decomposes on Ni clusters at a rate that is strongly dependent on particle size, especially for clusters below 5 nm in diameter. Previous works have shown that CO has a high dissociation rate on Ni at step edges [25] and sputter-damaged surfaces [26]. Table 1 shows clear trends in the evolution of desorption parameters with Ni coverage and CO exposure. Both the desorption energies and vibrational prefactors increase with increasing Ni coverage, and decrease with increasing CO exposure. For the lowest Ni coverage (0.2 ML), anomalous low vibrational prefactors are obtained. Based on this finding and the discussion above, it may be argued that dissociative adsorption of CO predominates at this coverage with small Ni nanostructures. In the case of high Ni coverage (2.9 ML), terrace atoms dominate and molecular adsorption predominates. This argument is then supported by higher vibrational prefactors. In the case of intermediate Ni coverage (0.56 ML), high values for vibrational prefactors are obtained for low CO exposure and low values for vibrational prefactors are obtained for higher CO exposures. This may be an indication that molecular adsorption of CO takes place initially, and subsequently, when all terrace sites are occupied the adsorption becomes dissociative. A comprehensive understanding why dissociative adsorption should result in lower desorption energies and thus lower desorption temperatures has not been reached. However, it may be conceivable that the interface between the nanoparticles and the muscovite mica substrate play a role in the desorption characteristics at low Ni coverage.

## 5. Conclusions

Three major components were observed in the CO TPD spectra from nickel-decorated muscovite mica. For a heating rate of 1 K/s major peaks were found near 250, 400 and 550 K. For samples with low amounts of Ni, about 0.2 ML, predominantly the low temperature peak was found. For samples with intermediate amount of Ni, about 0.6 ML, all three peaks were observed, whereas in the case of large Ni amounts, about 3.0 ML, only the high temperature peak was seen. The high temperature peak was assigned to desorption from terraces on the nickel particles, the intermediate peak was assigned to desorption from step sites, and the low temperature peak was assigned to lateral interactions between adsorbed CO molecules and possibly desorption from low-coordinated sites. Anomalous low values obtained for the vibrational prefactor is believed to be caused by partial dissociation of CO and edge distortion caused by adsorption in several near equivalent sites.

## Acknowledgements

This work was supported by the Research Council of Norway (RCN) under project no. NFR 250728.

## References

[1] A.T. Bell, The impact of nanoscience on heterogeneous catalysis, Science 299 (2003) 1688–1691, https://doi.org/10.1126/science.1083671.
[2] J. Carrazza, G.A. Somorjai, Structure sensitivity of catalytic reactions, Ind. Eng. Chem. Res. 25 (1986) 64–69, https://doi.org/10.1021/i100021a009.
[3] R.I. Masel, Principles of Adsorption and Reaction on Solid Surfaces, a Wiley-Interscience Publication, Wiley, 1996 URL https://books.google.no/books?id=cf9bR3MqgIIC.
[4] R. Davda, J. Shabaker, G. Huber, R. Cortright, J. Dumesic, Aqueous-phase reforming of ethylene glycol on silica-supported metal catalysts, Appl. Catal. B Environ. 43 (1) (2003) 13–26, https://doi.org/10.1016/S0926-3373(02)00277-1.
[5] G.A. Somorjai, Introduction to Surface Chemistry and Catalysis, Wiley, New York, 1994.
[6] Z.-P. Hu, C.-C. Weng, G.-G. Yan, X.-W. Lv, Z.-Y. Yuan, Ni nanoparticles supported on mica for efficient decomposition of ammonia to $CO_x$-free hydrogen, Int. J. Hydrog. Energy 20 (2018) 9663–9676, https://doi.org/10.1016/j.ijhydene.2018.04.029.
[7] P. Li, B. Wen, F. Yu, M. Zhu, X. Guo, Y. Han, L. Kang, X. Huang, J. Dan, F. Ouyang, B. Dai, High efficient nickel/vermiculite catalyst prepared via microwave irradiation-assisted synthesis for carbon monoxide methanation, Fuel 171 (2016) 263–269, https://doi.org/10.1016/j.fuel.2015.12.076.
[8] J. Gao, C. Jia, J. Li, M. Zhang, F. Gu, G. Xu, Z. Zhong, F. Su, Ni/$Al_2O_3$ catalysts for CO methanation: effect of $Al_2O_3$ supports calcined at different temperatures, J. Energy Chemistry 22 (2013) 919–927, https://doi.org/10.1016/S2095-4956(14)60273-4.
[9] H. Poppa, A.G. Elliot, The surface composition of mica substrates, Surf. Sci. 24 (1971) 149, https://doi.org/10.1016/0039-6028(71)90225-1.
[10] F. Ostendorf, C. Schmitz, S. Hirth, A. Kühnle, J.J. Kolodziej, M. Reichling, How flat is an air-cleaved mica surface? Nanotechnology 19 (2008) 305705, , https://doi.org/10.1088/0957-4484/19/30/305705.
[11] D.A. King, Thermal desorption from metal surfaces: a review, Surf. Sci. 47 (1975) 384–402, https://doi.org/10.1016/0039-6028(75)90302-7.
[12] J.B. Miller, H.R. Siddiqui, S.M. Gates, J.N. Russell Jr., J.T. Yates Jr., J.C. Tully, M.J. Cardillo, Extraction of kinetic parameters in temperature programmed desorption: a comparison of methods, J. Chem. Phys. 87 (1987) 6725–6732, https://doi.org/10.1063/1.453409.
[13] B. Meng, W.H. Weinberg, Monte-Carlo simulations of temperature programmed desorption spectra, J. Chem. Phys. 100 (1994) 5280, https://doi.org/10.1063/1.467192.
[14] M. Juel, S. Raaen, Thermal desorption of CO from Mo(110), Philos. Mag. 83 (2003) 2475, https://doi.org/10.1080/1478643031000116023.
[15] S. Raaen, A. Ramstad, Monte-Carlo simulations of thermal desorption of adsorbed molecules from metal surfaces, Energy 30 (2005) 821–830, https://doi.org/10.1016/j.energy.2004.03.101.
[16] C. Benndorf, L. Meyer, CO adsorption on stepped Ni(111) surfaces, J. Vac. Sci. Technol. A 8 (1990) 2677–2681, https://doi.org/10.1116/1.576693.
[17] C. Benndorf, L. Meyer, CO adsorption on Ni(551), Surf. Sci. 251 (1991) 872–876, https://doi.org/10.1016/0039-6028(91)91115-E.
[18] D. Doering, J. Dickinson, H. Poppa, UHV studies of the interaction of CO with small supported metal particles, NiMica, J. Catal. 73 (1982) 91–103, https://doi.org/10.1016/0021-9517(82)90084-7.
[19] R.A. van Santen, M. Neurock, Molecular Heterogeneous Catalysis, Wiley-VCH, 2006.
[20] G.C. Bond, Small particles of the platinum metals, Platin. Met. Rev. 19 (4) (1975) 126–134.
[21] C.A. de Araujo Filho, D.Y. Murzin, A structure sensitivity approach to temperature programmed desorption, Appl. Catal. A Gen. 550 (2018) 48–56, https://doi.org/10.1016/j.apcata.2017.11.001.
[22] G. Wedler, H. Papp, G. Schroll, Adsorption of carbon monoxide on polycrystalline nickel films, Surf. Sci. 44 (1974) 463–479, https://doi.org/10.1016/0039-6028(74)90131-9.
[23] H. Madden, G. Ertl, Decomposition of carbon monoxide on a (110) nickel surface, Surf. Sci. 35 (1973) 211–226, https://doi.org/10.1016/0039-6028(73)90215-X.
[24] W. Erley, H. Wagner, Thermal decomposition of CO on a stepped Ni surface, Surf. Sci. 74 (2) (1978) 333–341, https://doi.org/10.1016/0039-6028(78)90030-4.
[25] H. Nakano, S. Kawakami, T. Fujitani, J. Nakamura, Carbon deposition by disproportionation of CO on a Ni(977) surface, Surf. Sci. 454-456 (2000) 295–299, https://doi.org/10.1016/S0039-6028(00)00265-X.
[26] C. Astaldi, A. Santoni, F.D. Valle, R. Rosei, Co dissociation and recombination reactions on Ni(100), Surf. Sci. 220 (1989) 322–332, https://doi.org/10.1016/0039-6028(89)90235-5.